ACS APPLIED MATERIALS & INTERFACES

Research Article

www.acsami.org

Photovoltaic Device Performance of Single-Walled Carbon Nanotube and Polyaniline Films on n-Si: Device Structure Analysis

Shawn E. Bourdo,*[,†] Viney Saini,[†] Jimmy Piron,[‡] Ismael Al-Brahim,[‡] Cyril Boyer,[‡] Julian Rioux,[‡] Venugopal Bairi,[§] Alexandru S. Biris,[†,⊥] and Tito Viswanathan[§]

[†]Nanotechnology Center, [§]Department of Chemistry, and [⊥]Department of Applied Science, University of Arkansas at Little Rock, Little Rock, Arkansas 72204, United States

[‡]Ecole d'Ingenieurs du CESI-EIA, La Couronne, France

ABSTRACT: In this paper, we explore the use of two organic materials that have been touted for use as photovoltaic (PV) materials: inherently conducting polymers (ICPs) and carbon nanotubes (CNTs). Due to these materials' attractive features, such as environmental stability and tunable electrical properties, our focus here is to evaluate the use of polyaniline (PANI) and single wall carbon nanotube (SWNT) films in heterojunction diode devices. The devices are characterized by electron microscopy (film morphology), current−voltage characteristics (photovoltaic behavior), and UV/visible/NIR spectroscopy (light absorption). We have found that both PANI and SWNT can be utilized as photovoltaic materials in a simple bilayer configuration with n-type Silicon: n-Si/PANI and n-Si/SWNT. It was our aim to determine how photovoltaic performance was affected utilizing both PANI and SWNT layers in multilayer devices: n-Si/PANI/SWNT and n-Si/SWNT/PANI. The short-circuit current density increased from 4.91 mA/cm^2 (n-Si/PANI) to 12.41 mA/cm^2 (n-Si/PANI/SWNT), while an increase in power conversion efficiency by ∼91% was also observed. In the case of n-Si/SWNT/PANI and its corresponding device control (n-Si/SWNT), the short-circuit current density was decreased by an order of magnitude. The characteristics of the device were affected by the architecture and the findings have been attributed to the more effective transport of holes from the PANI to SWNT and less effective transport of holes from PANI to SWNT in the respective multilayer devices.

KEYWORDS: *carbon nanotubes, polyaniline, thin films, photovoltaic devices, hybrid solar cells*

1. INTRODUCTION

Photovoltaic (PV) devices have been an area of major focus for scientists in recent years. The impetus is the impending energy crisis coupled with the fact that new materials for affordable solar cell technologies are being discovered in numerous laboratories. The basic photovoltaic cell consists of either a p−n junction or Schottky junction (metal-semiconductor) and is most commonly achieved using doped inorganic semiconductor materials, e.g., silicon and germanium.[1] Recently, carbon nanostructures and polymers have been utilized in p−n junction and Schottky junction based solar cells.[2−4] Novel materials are continually being discovered for use in traditional layered heterojunction diode devices and bulk heterojunction organic PV devices. The necessity for cheaper routes to renewable energy devices and an increase in device efficiencies are two major forces in the area of PV research. Organic materials have the potential to drive down the production costs of solar cells due to ease of processing by using techniques such as inkjet printing, spray deposition and spin-coating.[5] Most of the materials research focus for organic photovoltaics (OPV) has been applied to either bulk heterojunction devices or dye-sensitized solar cells (DSSC)[6] whereas the use of graphitic nanomaterials was proposed to enhance the stability, and the electro-optical properties of the photoactive materials.[7−9]

In this report, we explore two organic materials that have been touted for use as photovoltaic materials: inherently conducting polymers (ICPs) and carbon nanotubes (CNTs).[10] The ability to tune the electrical properties of ICPs and CNTs provides a plethora of variables to study when incorporating these materials into photovoltaic devices. Carbon nanotubes exhibit a range of electronic properties based on the type of nanotube (single-, double-, multiwall, etc.) with excellent transport properties[11−14] − hole mobilities have been reported between 1 × 10^2 and 1 × 10^5 cm^2/(V s) and conductivities as high as 1 × 10^5 S/cm. However, the characteristics of CNTs are not as easily tunable as the conducting polymers. For example PANI can exhibit electrical conductivities[15−17] over many orders of magnitudes (up to 1,300 S/cm in doped samples) and hole mobilities[18,19] range from 1 × 10^{-3} to 1 × 10^{-1} cm^2/(V s) based on dopant type and amount, synthesis and processing conditions, and oxidation state. Polyaniline (PANI) is an ICP that is extensively utilized because of its facile synthesis, environmental stability, and the aforementioned tunable electrical properties.[20] Polyaniline has been reported to function as a hole transport layer in OPVs,[21−23] as well as charge generation and collection layer in p−n heterojunction (PANI/n-Si) and Shottky junction (PANI/GaN) solar cells with promising results.[4,24,25] PANI is an excellent candidate for low-cost photovoltaic material, because it can be processed into solution,[15,26,27] which allows for deposition by inkjet printing, spray-deposition, spin-coating, etc. There is also a focus on utilizing carbon-nanotubes in solar cells, including transparent conducting electrodes and active layers.[28,29] The high aspect ratio and surface area of CNTs provide excellent charge

Received: October 17, 2011
Accepted: December 26, 2011
Published: December 26, 2011

collection and transportation properties, allowing them to be useful in many electronic applications.[30,31]

Our focus here is to evaluate for the very first time, to the best of our knowledge, the use of PANI and single-walled carbon nanotubes (SWNTs) in multilayer heterojunction devices. The genesis of this work came about during discussions regarding easily processable materials that could be integrated on the top side of traditional PV devices (e.g., c-Si-, mc-Si-, and a-Si-based solar cells). Once the characteristics of these simple devices are understood, they can be utilized in more complex structures, such as multijunction cells. For these initial studies, we have investigated the effects of layering both PANI and SWNT films onto n-type Si in two different geometries: (i) n-type silicon substrate has been coated with a layer of PANI followed by deposition of SWNT films (n-Si/PANI/SWNT), (ii) n-type silicon substrate has been coated with SWNT films and then covered by a layer of PANI film (n-Si/SWNT/PANI). For comparison, two separate devices with a single layer of either PANI or SWNT (n-Si/PANI and n-Si/SWNT) have also been fabricated and characterized. Special attention was provided during fabrication of all the devices, to keep the SWNT film and PANI film deposition conditions same throughout the device fabrication process, so as to achieve approximately the same film thickness for all the devices. We have evaluated the devices by scanning electron microscopy (film morphology), current−voltage characteristics (photovoltaic behavior), and UV/visible/NIR spectroscopy (light transmission). While the power conversion efficiencies of the single layered PV devices (n-Si/PANI and n-Si/SWNT) are modest, an almost 2-fold increase in power conversion efficiency is achieved for the device structure n-Si/PANI/SWNT. Such kind of novel approaches could result in the development of organic photovoltaic devices with novel configurations and would result in enhanced optical conversion capabilities.

2. EXPERIMENTAL DETAILS

2.1. Materials. Aniline was obtained from Fisher Scientific and doubly distilled prior to use. 10-Camphorsulfonic Acid (98%, Aldrich), *m*-cresol (99+%, Aldrich), dimethylformamide (DMF) (anhydrous, Aldrich), concentrated hydrofluoric acid (47−51%, Fisher Scientific), hydrogen peroxide (35%, Fisher Scientific), concentrated NH_4OH (28−30%, Aldrich), and KBr (99+% FTIR grade, Aldrich) were used as received. Single-walled carbon nanotubes were purchased from Southwest Nanotechnologies and used as received. Silicon wafers were purchased from WRS Materials and were treated with aqueous peroxide/hydroxide (1:1:5, 35% H_2O_2:conc NH_4OH:deionized water) to remove any organic contaminants, followed by dilute HF (1:30, conc. HF:deionized water) to remove the native SiO_2 prior to deposition of SWNT and PANI films.

2.2. Synthesis and Processing of Polyaniline. Polyaniline (PANI) was synthesized by the MacDiarmid method.[32] Specifically, a 1 mL aliquot of aniline was added to 25 mL of 1 M HCl in a jacketed beaker and stirred with a magnetic stir-bar. The solution was then cooled to between 0 and 2 °C using ice water recirculated with a pump. The reaction was allowed to proceed overnight, and the solid polyaniline precipitate (emeraldine salt) was isolated by vacuum filtration through a Whatman 4 filter paper. The solids were then washed with deionized water.

To obtain the emeraldine base form of PANI for solution processing, we initially washed the wetcake with 1 M NH_4OH and then stirred in 0.1 M NH_4OH overnight to complete the dedoping process. The solids were isolated by vacuum filtration through a Whatman 4 filter paper. The solid wetcake (emeraldine base) was washed with deionized water until the filtrate was at neutral pH. The samples were dried overnight under vacuum.

Doped polyaniline solutions were prepared by mixing 0.064 g emeraldine base with 0.069 g camphorsulfonic acid as a dopant and 6.3 g *m*-cresol as a solvent. This mixture was stirred vigorously overnight, and the solids were centrifuged out. The supernatant solution was then used in the fabrication of our devices. PANI devices were spin-coated at 600 rpm and the solvent evaporated in a vacuum oven at ∼80 °C.

2.3. Preparation of SWNT Films. The SWNTs were first dispersed in DMF (10 mg/mL) by using bath sonication technique for a total of 12 h in four 3 h intervals, and the solids were centrifuged out. The remaining supernatant solution was then removed and sonicated for another 6 h and was used for device fabrication. The devices were prepared by spraying SWNTs dispersion in DMF by airbrush deposition technique at 150 °C. Glass slides were placed side by side with the silicon substrates, and SWNTs were sprayed simultaneously on both substrates in order to achieve similar SWNT film thickness. The SWNT film deposited on glass substrate was employed for optical transparency measurements.

2.4. Fabrication of Photovoltaic Devices. We have investigated a new type of solar cell with device architecture similar to previous work performed on n-Si/SWNTs heterojunction solar cells.[9] In this work, we used polyaniline (PANI), which is a p-type inherently conducting polymer, as a hole conducting material in n-Si/PANI heterojunction solar cells. The four different solar cell device configurations are summarized below:

(1) PANI film spin-coated (approximate thickness 115 nm from SEM analysis, 81% transparent at 550 nm) over n-type silicon. Device Structure: n-Si/PANI
(2) SWNTs film (approximate thickness 100 nm from SEM analysis, 51% transparent at 550 nm wavelength) deposited by airbrush deposition technique over n-type silicon. Device Structure: n-Si/SWNTs
(3) PANI film spin-coated over n-type silicon followed by deposition of SWNT film by airbrush technique. Device Structure: n-Si/PANI/SWNTs.
(4) SWNT film deposited over n-type silicon and followed by spin-coating with PANI film. Device Structure: n-Si/SWNT/PANI.

2.5. Characterization Techniques. *2.5.1. Scanning Electron Microscopy (SEM).* Scanning electron micrograph images were taken by using a JEOL 7000F SEM in the secondary electron mode under an accelerating voltage of 15.0 kV and current of 74 μA. The samples were imaged without any special surface treatment. Images were taken from the top and side views for all the samples.

2.5.2. Structural Characterization (Infrared and Raman Spectroscopy). Infrared and Raman spectroscopy were employed to evaluate the polyaniline and carbon nanotubes, respectively, used in the fabrication of PV devices. A Nicolet MAGNA 550 FTIR was used to analyze the synthesized polyaniline prior to solution processing. A few milligrams of powdered PANI samples were combined with KBr and ground in a mortar and pestle. The mixture was then pressed into a pellet and the IR transmission was measured between 4000 and 400 cm^{-1}.

Raman scattering study of the SWNTs in powder form was performed at room temperature using a Horiba Jobin Yvon LabRam HR800 equipped with a charge-coupled detector, a spectrometer with a grating of 600 lines/mm and a He−Ne laser (633 nm) as excitation source. The laser beam intensity measured at the sample was kept at 2 mW. The microscope focused the incident beam to a spot size of <0.01 mm^2, and the backscattered light was collected 180° from the direction of incidence. Raman shifts were calibrated with a silicon wafer at a peak of 521 cm^{-1}.

2.5.3. Optical Spectroscopy. A Shimadzu UV-3600 UV/visible/NIR spectrometer with three detectors was used for transmission measurements from 250 to 1300 nm at 1 nm intervals and medium scan rate. Scans were performed on thin films of nanotubes and polyaniline on glass substrate prepared under identical conditions to the films prepared on n-Si substrate.

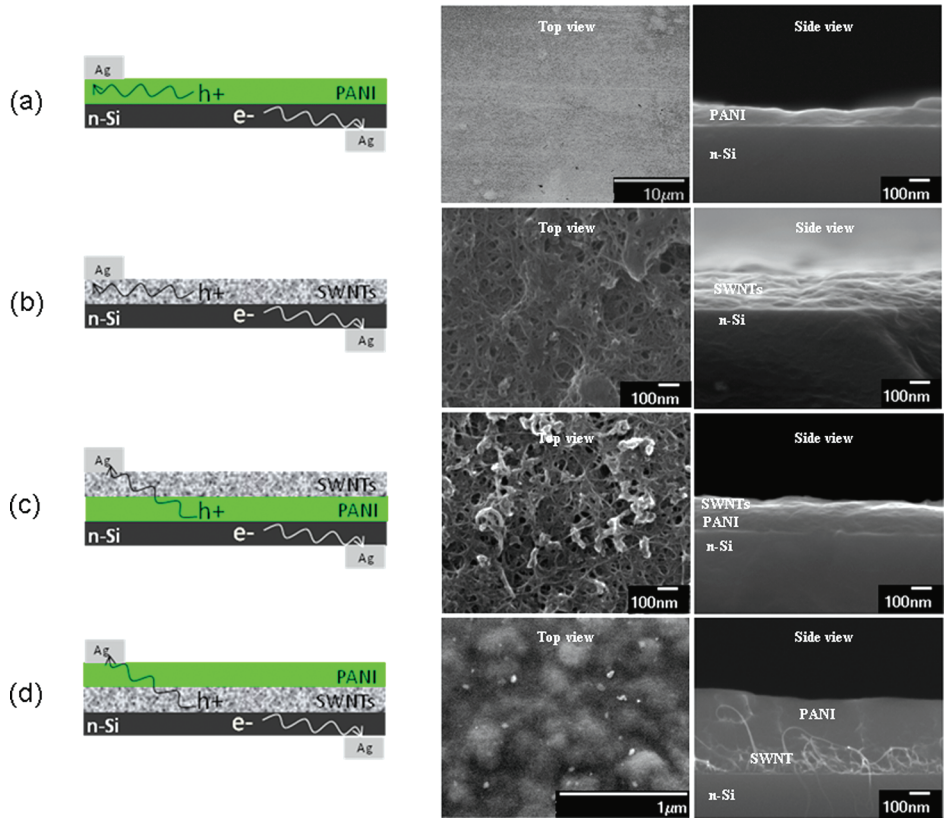

Figure 1. Device schematics (left) and scanning electron micrographs (right) for (a) n-Si/PANI, (b) n-Si/SWNTs, (c) n-Si/PANI/SWNTs, and (d) n-Si/SWNT/PANI devices.

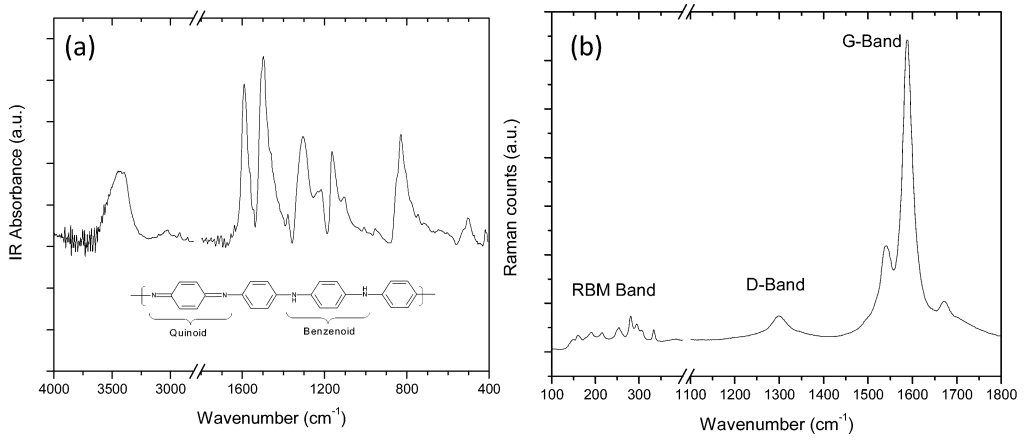

Figure 2. (a) FTIR spectra of the emeraldine base form of polyaniline, inset shows tetrameric unit of polyaniline; and (b) Raman spectrum of SWNT powder sample.

2.5.4. Current–Voltage Studies of PV cells. The current–voltage (IV) characteristics of solar cell devices (active areas of devices were approximately 0.01 cm^2) were tested under dark and illuminated conditions (AM 1.5, 100mW/cm^2) using a class-B small area solar simulator (PV Measurements Inc.) and Keithley 2400 Sourcemeter. Current–voltage scans were performed from −1 V to +1 V with a step of 4 mV using a Labview program.

3. RESULTS AND DISCUSSION

3.1. Electron Microscopy. Electron microscopy was employed to evaluate the films' thickness and their morphologies. Figure 1 shows the four device schematics and SEM top view and side view images of the four device architectures. Each view of the layers provides different morphological information. The two materials under investigation have different film-forming properties as evidenced by the SEM images of the pristine SWNT and PANI on n-Si substrate. The spin-coated polyaniline solutions result in films that are very uniform and are in intimate contact with the silicon substrate. The airbrushed nanotubes are not ideal "films" as such because of their porous nature, and may limit the ability to form a uniform junction across the silicon substrate.

The side view gives a unique look into the layered structure of the devices, and the most dramatic image is that of the n-Si/SWNT/PANI device (Figure 1d). This image gives a better indication of the morphology of SWNT than the image of n-Si/SWNTs alone since the PANI provides some contrast with the

dx.doi.org/10.1021/am201426y | ACS Appl. Mater. Interfaces 2012, 4, 363–368

SWNTs. The PANI diffuses between the SWNT film pores and results in better interface between PANI and SWNTs. Figure 1d with side view of n-Si/SWNT/PANI device does not provide true thickness of PANI film. The PANI film was observed to bulge under the electron beam. Therefore, this particular image shown here was not used to estimate thickness of PANI film.

3.2. Structural Characterization. The materials used for device fabrication were analyzed by structural spectroscopy: Infrared and Raman spectroscopy. Polyaniline exhibits several prominent features when probed by infrared (IR) spectroscopy providing insight into degree of oxidation. The two most prominent IR-bands are at 1497 and 1590 cm^{-1} and stretching modes associated with the benzenoid and quinoid structural units (see inset of Figure 2a), respectively. The intensity of the two bands is a measure of the polymer oxidation state; the slightly larger intensity of the 1500 cm^{-1} band is indicative of polyaniline in the emeraldine (half-oxidized) form and is similar to spectra in the literature.[33,34] Other noticeable bands appear at ~3400 cm^{-1} (N−H stretch), 1378 (C−C stretch + C−H bend), 1303 cm^{-1} (C−H bend), 1219 cm^{-1} (C−N stretch + ring deformation), 1164 cm^{-1} (C−H bend), and 829 cm^{-1} (para-disubstituted benzene).[33]

Raman spectroscopy is a very useful technique to characterize and study the structural features of carbon nanotubes. The Raman spectrum in Figure 2b of a powder SWNT sample shows three main bands, radial breathing mode (RBM), D-band and G-band. The RBM, in the range 100−500 cm^{-1}, is the characteristic Raman scattering of single-walled carbon naotubes. These peaks originate due to vibration and stretching of SWNTs along the diameters under laser excitation. The diameter of SWNTs can be closely estimated by using the formula below[35]

$$\omega_{RBM}\ (cm^{-1}) = \frac{\alpha}{d\ (nm)} + a$$

where ω_{RBM} is the wavenumber, d is diameter, and α = 234 cm^{-1} and a =10 are constants.

The G-band observed at 1588 cm^{-1} is attributed to the in-plane stretching mode of ordered crystalline graphite like structures. It originates from the splitting of the E_{2g} in graphite-like materials and is a characteristic mode of SWNTs. The D-band observed at 1298 cm^{-1} is assigned to the disorder and defects in carbon structures. The ratio (G/D) of the area under G and D band estimates the crystallinity of SWNTs. A high G/D ratio means low defect sites, less impurities and better crystalline quality of SWNTs.[8,36]

3.3. Optical Transmission. Ultraviolet−visible−near-infrared (UV−vis−NIR) spectroscopy was performed in order to determine the transparency of individual PANI and SWNTs films. In preparing our solar cells, every attempt was made to keep the SWNTs film thickness the same for all the devices; this is also true for PANI films. Figure 3 shows representative UV−vis−NIR spectra of the PANI and SWNTs films. The results show that each material has its own specific absorption bands.

Through most of the visible region (400−700 nm), PANI has greater than 50% transparency with a maximum (approximately 82%) and minimum (approximately 31%) transmission at 520 nm and 444 nm, respectively. The electronic transition at 444 nm is due to the polaron−π^* excitation of electrons. The continuous increase in spectral absorbance >600 nm is indicative of the electrically conductive,

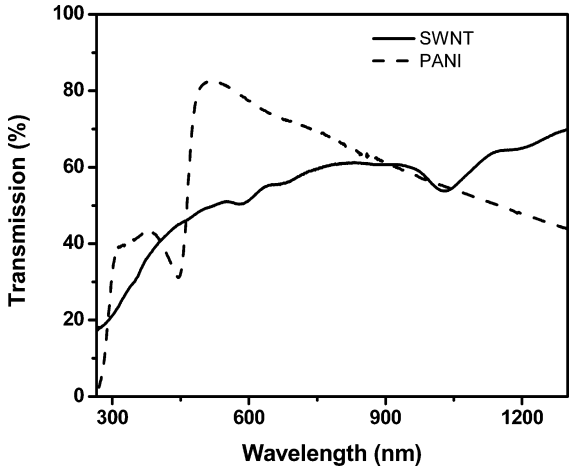

Figure 3. UV−visible−NIR transmission spectra of SWNT (solid line) and PANI film (dashed line).

doped, form of PANI (emeraldine salt) and is generally referred to as a free carrier tail (Drude absorption).[17] The transparency in the visible region for the SWNT films lies between 40% and 60% with 51% transparency as measured at 550 nm. The spectra convey that PANI films provide better light transmission in the visible region than the SWNTs film. In the device where SWNTs are utilized as a hole collection layer (n-Si/PANI/SWNT), the less transparent SWNT film blocks approximately 50% of the radiation from reaching the n-Si/PANI heterojunction, thus decreasing the open-circuit voltage (as shown in Table 1) while at the same time providing an

Table 1. Summary of Device Characteristics (maximum values are bold)

sample name	V_{OC} (V)	J_{SC} (mA/cm^2)	FF	efficiency (%)
n-Si/PANI	**0.354**	4.91	0.185	0.322
n-Si/SWNT	0.193	4.24	0.255	0.209
n-Si/PANI/SWNT	0.189	**12.41**	**0.262**	**0.614**
n-Si/SWNT/PANI	0.194	0.67	0.154	0.0201

efficient pathway for free charges to be collected at the electrodes.

3.4. Illuminated and Dark Current−Voltage Characteristics. This research work has been focused on utilizing air-stable, p-type materials like PANI and SWNTs in hybrid solar cells. This report combines the two approaches to fabricate devices utilizing both materials, where the final architecture results in a multilayered device. These multilayer devices are compared with single layered heterojunctions. Previous reports have demonstrated the charge generation capacities of PANI- and SWNT-silicon based solar cells.[9,37,38] This report focus mainly on the charge generation versus the efficient charge collection and transportation of charges to the electrodes. Figure 4 displays a representative photovoltaic response of one of the fabricated device (n-Si/PANI/SWNT). The current−voltage (I−V) characteristics of solar cell devices were tested under dark and illuminated conditions (AM 1.5, 100mW/cm^2) using a Keithley 2400 Sourcemeter.

The solar cell device performance figure of merits, open-circuit voltage (V_{oc}), short-circuit current density (J_{sc}), fill factor (FF), and power conversion efficiency (η) are summarized in Table 1 for all the devices. The n-Si/PANI/SWNT device

dx.doi.org/10.1021/am201426y | ACS Appl. Mater. Interfaces 2012, 4, 363−368

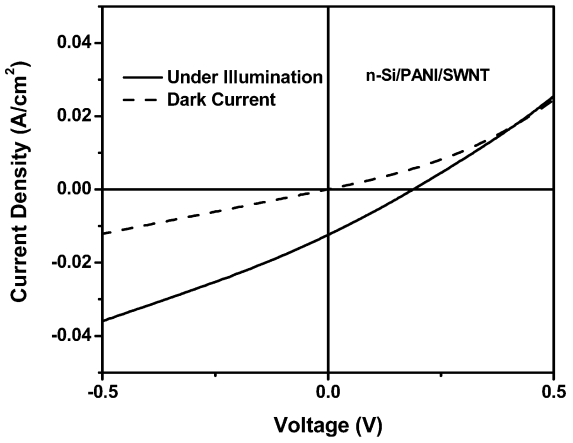

Figure 4. Representative illuminated and dark current−voltage characteristic trace (device structure shown is n-Si/PANI/SWNTs).

shows much higher short-circuit current density when compared to the other devices and also the highest efficiency. When the solar cells are illuminated, the photoexcited charge carriers dissociate into free electrons and holes at the n-Si/PANI heterojunction. When the photoexcited free charge carriers are close to the pn-junction (n-Si and PANI in this case), free electrons are transported through n-Si to the cathode, and the holes are swept away from the junction through the PANI layer. Owing to the p-type nature of SWNTs, they can act as efficient hole collectors. The SWNT film deposited over PANI collects the charges from the PANI film and transports them to the anode because of their high charge transportation capabilities.

In our studies, we found that comparative analysis of single-layer and multilayer devices are quite intriguing. In the n-Si/PANI device, we have observed a high open-circuit voltage (0.354 V), which is due to the reason that PANI film creates a uniform and homogeneous heterojunction with n-Si, with little blockage of the incoming light in the visible region of the spectrum. Therefore, PANI film deposited over n-Si can extract holes effectively from the junction, but the device also exhibits low fill factor (0.185) because of poor charge transportation through PANI film. On the other hand, n-Si/SWNT device shows low open-circuit voltage (0.193 V), likey due to the blockage of incoming light (approximately 50% transparent throughout the visible region). It is well-known in photoelectric materials[39,40] and reported by many groups that light intensity plays an important role in the observed open-circuit voltage of a photovoltaic device.[41−43] This device shows better fill-factor (0.255) and similar short-circuit current densities (4.24 mA/cm^2) compared to that of n-Si/PANI device. Even though the open circuit voltage is low due to the blockage of incoming radiation, a larger percentage of holes (compared to PANI) are effectively transported through the SWNT film because of high charge collection and transportation properties of SWNTs. Next, we have tried to incorporate the PANI and SWNTs films in multilayer heterojunction design over n-Si substrate.

The ability of PANI in creating uniform and homogeneous heterojunction over n-Si substrate and, charge collection and transportation properties of SWNTs were the two driving forces in developing the multilayer heterojunction solar cells. Two multilayer heterojunction device architectures were fabricated and analyzed; n-Si/PANI/SWNT and n-Si/SWNT/PANI. As summarized in Table 1, incorporating SWNT film over PANI has more than doubled the short-circuit current density, from 4.91 mA/cm^2 for n-Si/PANI device to 12.41 mA/cm^2 for n-Si/PANI/SWNTs device. The SWNT film provides a semitransparent conducting "mat" over the whole device area through which charges are collected and transported to the anode, thereby increasing the current density, fill factor and hence power conversion efficiency. While the SWNT film on top of PANI increases the efficiency of the device, the open circuit voltage decreases by almost half (0.354 to 0.189 V), because of the reduction of light reaching the n-Si/PANI junction. For the devices n-Si/SWNT and n-Si/SWNT/PANI, the SWNTs film creates a p-n junction with n-Si. Because the PANI film is relatively transparent in the visible region and no change in open circuit voltage was observed, however, the current density drops an order of magnitude for n-Si/SWNT/PANI device. This observation leads to the finding that holes were unable to transport from SWNTs to PANI as efficiently as from PANI to SWNTs. Therefore, PANI as a top layer reduces the short-circuit current density due to poor transportation of holes from SWNTs to PANI in the n-Si/SWNT/PANI device. In our opinion, by comparing the short circuit current densities obtained in n-Si/PANI/SWNT and n-Si/SWNT/PANI architectures, an efficient hole transportation occurs from PANI to SWNTs but not in reverse direction, likely because of the band alignment and hole mobilites of these two materials.

In summary, out of all the device architectures reported here, n-Si/PANI/SWNT is the most efficient device architecture. Even though the open-circuit voltage of this device decreased by ∼47% due to blockage of light by the SWNT film, the short-circuit current density increased by ∼150%, fill factor by ∼42%, and power conversion efficiency by ∼91%. This increase is due to the formation of uniform heterojuction between PANI and n-Si, coupled with the proficient exchange of charges (holes) from PANI to the SWNT "mat" and subsequent transportation to the anode that results in the highest performing solar cell device architecture that is studied here.

4. CONCLUSIONS

In this report, we have demonstrated that both PANI and SWNTs are viable materials for PV devices and the efficiency of a PV device can be improved by utilizing both the materials. The n-Si/PANI device exhibits the highest open-circuit voltage (0.354 V) as compared to the n-Si/SWNT device. The superior V_{OC} is due to the uniform PANI film being more transparent throughout the visible region of the solar spectrum, whereas the SWNT film prevents about 50% of the light from reaching the heterojunction. In multilayer heterojunction devices, when SWNTs are utilized as a top layer over PANI (i.e., n-Si/PANI/SWNT device), the overall efficiency of the solar cell increases because the SWNTs serve as an effective hole collection "network" on top of the device. The device architecture n-Si/SWNT/PANI shows very low photovoltaic response due to the decreased current density and stems from less efficient hole transport from SWNT to PANI film. The best device architecture studied in this report is n-Si/PANI/SWNT. The performance of this device can be further optimized by varying the PANI and SWNT film thickness, so that a balance of electrical properties of PANI and SWNT along with SWNT transparency is achieved resulting in higher efficiency. The tunable electrical properties of both PANI and SWNT through doping should thus lead to unique device structures in future studies.

AUTHOR INFORMATION

Corresponding Author

*E-mail: sxbourdo@ualr.edu.

ACKNOWLEDGMENTS

Financial support from the Arkansas Science & Technology Authority (Grant 08-CAT-03), the Department of Energy (DE-FG36-06GO86072), and the National Science Foundation (NSF/EPS-1003970) is greatly appreciated. The editorial assistance of Dr. Marinelle Ringer is also acknowledged.

REFERENCES

(1) Rockett, A., *The Materials Science of Semiconductors*; Spinger: New York, 2008; p 622.
(2) Jia, Y.; Wei, J.; Wang, K.; Cao, A.; Shu, Q.; Gui, X.; Zhu, Y.; Zhuang, D.; Zhang, G.; Ma, B.; Wang, L.; Liu, W.; Wang, Z.; Luo, J.; Wu, D. *Adv. Mater.* **2008**, *20*, 4594−4598.
(3) Li, X.; Zhu, H.; Wang, K.; Cao, A.; Wei, J.; Li, C.; Jia, Y.; Li, Z.; Li, X.; Wu, D. *Adv. Mater.* **2010**, *22*, 2743−2748.
(4) Matsuki, N.; Irokawa, Y.; Nakano, Y.; Sumiya, M. *Sol. Energy Mater. Sol. Cells* **2011**, *95*, 284−287.
(5) Brabec, C. J.; Durrant, J. R. *MRS Bull.* **2008**, *33*, 670−675.
(6) Hoppe, H.; Sariciftci, N. S. *J. Mater. Res.* **2004**, *19* (7), 1924−1945.
(7) Bourdo, S.; Li, Z.; Biris, A. S.; Watanabe, F.; Viswanathan, T.; Pavel, I. *Adv. Funct. Mater.* **2008**, *18* (3), 432−440.
(8) Saini, V.; Li, Z.; Bourdo, S.; Dervishi, E.; Xu, Y.; Ma, X.; Kunets, V. P.; Salamo, G. J.; Viswanathan, T.; Biris, A. R.; Saini, D.; Biris, A. S. *J. Phys. Chem. C* **2009**, *113* (19), 8023−8029.
(9) Li, Z.; Kunets, V. P.; Saini, V.; Xu, Y.; Dervishi, E.; Salamo, G. J.; Biris, A. R.; Biris, A. S. *ACS Nano* **2009**, *3* (6), 1407−1414.
(10) Dervishi, E.; Li, Z.; Xu, Y.; Saini, V.; Biris, A. R.; Lupu, D.; Biris, A. S. *Part. Sci. Technol.* **2009**, *27*, 107−125.
(11) Martel, R.; Schmidt, T.; Shea, H. R.; Hertel, T.; Avouris, P. *Appl. Phys. Lett.* **1998**, *73* (17), 2447−2449.
(12) Durkop, T.; Kim, B. M.; Furher, M. S. *J. Phys.: Condens. Matter* **2004**, *16*, R553−R580.
(13) Durkop, T.; Getty, S. A.; Cobas, E.; Furher, M. S. *Nano Lett.* **2004**, *4* (1), 35−39.
(14) Kaiser, A. B. *Rep. Prog. Phys.* **2001**, *64*, 1−49.
(15) Hopkins, A. R.; Rasmussen, P. G.; Basheer, R. A. *Macromolecules* **1996**, *29* (24), 7838−7846.
(16) Lee, K.; Cho, S.; Park, S. H.; Heeger, A. J.; Lee, C.-W.; Lee, S.-H. *Nature* **2006**, *441* (7089), 65−68.
(17) Xia, Y.; Wiesinger, J. M.; MacDiarmid, A. G.; Epstein, A. J. *Chem. Mater.* **1995**, *7*, 443−445.
(18) Patil, R.; Harima, Y.; Yamashita, K.; Komaguchi, K.; Itagaki, Y.; Shiotani, M. *J. Electroanal. Chem.* **2002**, *518*, 13−19.
(19) Harima, Y.; Patil, R.; Yamashita, K.; Yamamoto, N.; Ito, S.; Kitani, A. *Chem. Phys. Lett.* **2001**, *345*, 239−244.
(20) MacDiarmid, A. G. *Synth. Met.* **1997**, *84* (1−3), 27−34.
(21) Bejbouji, H.; Vignau, L.; Maine, J. L.; Dang, M.-T.; Oualim, E. M.; Harmouchi, M.; Mouhsen, A. *Sol. Energy Mater. Sol. Cells* **2009**, *94* (2), 176−181.
(22) Tan, S.; Zhai, J.; Xue, B.; Wan, M.; Meng, Q.; Li, Y.; Jiang, L.; Zhu, D. *Langmuir* **2004**, *20*, 2934−2937.
(23) Valaski, R.; Muchenski, F.; Mello, R. M. Q.; Micaroni, L.; Roman, L. S.; Hummelgen, I. A. *J. Solid State Electrochem.* **2006**, *10*, 24−27.
(24) Wang, W.; Schiff, E. A. *App. Phys. Lett.* **2007**, *91*, 133504/1−133504/3.
(25) Wang, W.; Schiff, E.; Wang, Q. *J. Non-Cryst. Sol.* **2008**, *354*, 2862−2865.
(26) Reghu, M.; Cao, Y.; Moses, D.; Heeger, A. J. *Phys. Rev. B* **1993**, *47* (4), 1758−1764.
(27) Cao, Y.; Smith, P.; Heeger, A. J. *Synth. Met.* **1992**, *48* (1), 91−7.
(28) Lagemaat, J. v. d.; Barnes, T. M.; Rumbles, G.; Shaheen, S. E.; Coutts, T. J.; Weeks, C.; Levitsky, I.; Peltola, J.; Glatkowski, P. *Appl. Phys. Lett.* **2006**, *88*, 233503/1−233503/3.
(29) Pasquier, A. D.; Unalan, H. E.; Kanwai, A.; Miller, S.; Chhowalla, M. *Appl. Phys. Lett.* **2005**, *87*, 203511/1−203511/3.
(30) Bellucci, S. *Phys. Status Solidi C* **2005**, *38*, 34−47.
(31) Sgobba, V.; Guldi, D. M. *Chem. Soc. Rev.* **2009**, *38*, 165−184.
(32) Mattoso, L. H. C.; Manohar, S. K.; MacDiarmid, A. G.; Epstein, A. J. *J. Appl. Polym. Sci., Part A: Polym. Chem.* **1995**, *33* (8), 1227−1234.
(33) Quillard, S.; Louarn, G.; Lefrant, S.; Macdiarmid, A. G. *Phys. Rev. B: Condens. Matter* **1994**, *50* (17), 12496−12508.
(34) Fukuda, T.; Takezoe, H.; Ishikawa, K.; Fukuda, A.; Woo, H. S.; Jeong, S. K.; Oh, E. J.; Suh, J. S. *Synth. Met.* **1995**, *69* (1−3), 175−6.
(35) Dervishi, E.; Li, Z.; Watanabe, F.; Xu, Y.; Saini, V.; Biris, A. R.; Biris, A. S. *J. Mater. Chem.* **2009**, *19*, 3004−3012.
(36) Zhang, L.; Balzano, L.; Resasco, D. E. *J. Phys. Chem. B* **2005**, *109* (30), 14375−14381.
(37) Bourdo, S. E.; Saini, V.; Warford, B. A.; Prou, F.; Bairi, V.; Li, Z.; Biris, A. S.; Viswanathan, T. *Proc. Mater. Res. Soc. Symp. HH* **2010**, 1270-HH14−54.
(38) Li, Z.; Saini, V.; Dervishi, E.; Kunets, V. P.; Zhang, J.; Xu, Y.; Biris, A. R.; Salamo, G. J.; Biris, A. S. *Appl. Phys. Lett.* **2010**, *96*, 0331100/1−0331100/3.
(39) Wurfel, P. *Physics of Solar Cells: From Basic Principles to Advanced Concepts*, 2nd ed.; Wiley-VCH: Weinheim, Germany, 2009.
(40) Bube, R. H., *Photoelectronic Properties of Semiconductors*; Cambridge University Press: New York, 1992.
(41) Schilinsky, P.; Waldauf, C.; Hauch, J.; Brabec, C. J. *J. Appl. Phys.* **2004**, *95* (5), 2816−2819.
(42) Barker, J. A.; Ramsdale, C. M.; Greenham, N. C. *Phys. Rev. B* **2003**, *67*, 075205/1−075205/9.
(43) Yunaz, I. A.; Kasashima, S.; Inthisang, S.; Krajangsang, T.; Miyajima, S.; Yamada, A.; Konagai, M. *Proceedings of the 34th IEEE Photovoltaics Specialists Conference (PVSC)*; IEEE: Piscataway, NJ, 2009; pp 000153−000157.